Systems/Circuits

# Integration of Swimming-Related Synaptic Excitation and Inhibition by olig2$^+$ Eurydendroid Neurons in Larval Zebrafish Cerebellum

**Thomas C. Harmon,**[1,2] **David L. McLean,**[1,2] **and Indira M. Raman**[1,2]
[1]Northwestern University Interdepartmental Neuroscience Program, and [2]Department of Neurobiology, Northwestern University, Evanston, Illinois 60208

**The cerebellum influences motor control through Purkinje target neurons, which transmit cerebellar output. Such output is required, for instance, for larval zebrafish to learn conditioned fictive swimming. The output cells, called eurydendroid neurons (ENs) in teleost fish, are inhibited by Purkinje cells and excited by parallel fibers. Here, we investigated the electrophysiological properties of glutamatergic ENs labeled by the transcription factor *olig2*. Action potential firing and synaptic responses were recorded in current clamp and voltage clamp from olig2$^+$ neurons in immobilized larval zebrafish (before sexual differentiation) and were correlated with motor behavior by simultaneous recording of fictive swimming. In the absence of swimming, olig2$^+$ ENs had basal firing rates near 8 spikes/s, and EPSCs and IPSCs were evident. Comparing Purkinje firing rates and eurydendroid IPSC rates indicated that 1-3 Purkinje cells converge onto each EN. Optogenetically suppressing Purkinje simple spikes, while preserving complex spikes, suggested that eurydendroid IPSC size depended on presynaptic spike duration rather than amplitude. During swimming, EPSC and IPSC rates increased. Total excitatory and inhibitory currents during sensory-evoked swimming were both more than double those during spontaneous swimming. During both spontaneous and sensory-evoked swimming, the total inhibitory current was more than threefold larger than the excitatory current. Firing rates of ENs nevertheless increased, suggesting that the relative timing of IPSCs and EPSCs may permit excitation to drive additional eurydendroid spikes. The data indicate that olig2$^+$ cells are ENs whose activity is modulated with locomotion, suiting them to participate in sensorimotor integration associated with cerebellum-dependent learning.**

*Key words:* **cerebellar nuclei; Purkinje cell; locomotion; IPSC; parallel fiber; complex spike**

### Significance Statement

**The cerebellum contributes to movements through signals generated by cerebellar output neurons, called eurydendroid neurons (ENs) in fish (cerebellar nuclei in mammals). ENs receive sensory and motor signals from excitatory parallel fibers and inhibitory Purkinje cells. Here, we report electrophysiological recordings from ENs of larval zebrafish that directly illustrate how synaptic inhibition and excitation are integrated by cerebellar output neurons in association with motor behavior. The results demonstrate that inhibitory and excitatory drive both increase during fictive swimming, but inhibition greatly exceeds excitation. Firing rates nevertheless increase, providing evidence that synaptic integration promotes cerebellar output during locomotion. The data offer a basis for comparing aspects of cerebellar coding that are conserved and that diverge across vertebrates.**

Received Sep. 27, 2019; revised Feb. 12, 2020; accepted Feb. 26, 2020.

Author contributions: T.C.H., D.L.M., and I.M.R. designed the research; T.C.H., D.L.M., and I.M.R. analyzed the data; T.C.H., D.L.M., and I.M.R. wrote the paper; T.C.H., D.L.M., and I.M.R. edited the paper; T.C.H. performed the research.

This work was supported by National Institutes of Health Grant R37-NS39395 to I.M.R., Grant F31-NS095476 to T.C.H., and Grant R01-NS067299 to D.L.M. We thank Drs. Bruce Appel, Reinhard Köster, and Shin-ichi Higashijima for fish lines; Elissa Szuter for technical help maintaining the fish colony; and Drs. Sandeep Kishore and Marion Najac for helpful discussions and comments on the manuscript.

The authors declare no competing financial interests.

T.C. Harmon's present address: Department of Neurobiology, Duke University, 311 Research Drive, Durham, NC 27710.

Correspondence should be addressed to Indira M. Raman at i-raman@northwestern.edu.

https://doi.org/10.1523/JNEUROSCI.2322-19.2020



## Introduction

The cerebellum regulates behavior through the firing patterns of Purkinje target neurons, which include neurons of the cerebellar nuclei (CbN) in mammals and eurydendroid neurons (ENs) in fish. These target neurons fire spontaneously (Thach, 1968; Jahnsen, 1986; Raman et al., 2000), and synaptic inputs combine with intrinsic properties to dictate cerebellar output, generating firing rates that often correlate with kinematic components of movements (Thach, 1968; Armstrong and Edgley, 1984; McCormick and Thompson, 1984; Goodkin and Thach, 2003; Chen et al., 2016; Brown and Raman, 2018). Additionally,

optogenetically elevating the firing of cerebellar output neurons elicits motor activity, whereas suppressing firing interrupts ongoing movement (Witter et al., 2013; Heiney et al., 2014; Proville et al., 2014; Lee et al., 2015; ten Brinke et al., 2015; Sarnaik and Raman, 2018; Brown and Raman, 2018), demonstrating that the activity of cerebellar output neurons likely influences many motor behaviors.

Studies of larval zebrafish indicate that cerebellum-dependent behaviors are present as early as 5-6 d post-fertilization (dpf) (Aizenberg and Schuman, 2011; Ahrens et al., 2012; Matsui et al., 2014; Matsuda et al., 2017; Knogler et al., 2019). Electrophysiological recordings of their Purkinje cells reveal synaptic responses from granule cell parallel fibers and inferior olivary climbing fibers and swimming-related increases in firing rate (Matsui et al., 2014; Sengupta and Thirumalai, 2015; Scalise et al., 2016); both synaptic excitation and spiking change gradually during associative motor learning (Harmon et al., 2017). Since Purkinje cells generally strongly inhibit their targets, these observations raise the question of how inhibition combines and/or competes with excitatory signals to affect firing by ENs. Despite the central role of synaptic integration in cerebellar output neurons in determining cerebellar contributions to behavior, the responses of ENs during motor behaviors have not been measured directly. Among the factors likely to determine the attributes of synaptic integration and spiking by ENs include the convergence of Purkinje cells onto target neurons; the inhibition elicited by simple and complex spikes; the relative magnitude and kinetics of IPSCs and EPSCs; and the extent to which inhibition and excitation are each modulated by motor commands associated with behavior.

As in mammals, Purkinje target neurons in fish are heterogeneous. A subset of putative ENs express the transcription factor olig2, whereas others express calretinin (Castro et al., 2006; McFarland et al., 2008; Bae et al., 2009; Matsui et al., 2014). Here, we have made current- and voltage-clamp recordings of olig2$^+$ ENs in immobilized larval zebrafish while monitoring fictive swimming. Multiple lines of evidence suggested that ENs receive input from an average of two Purkinje cells. Additionally, despite the great differences in simple and complex spike magnitude, IPSC amplitude was not correlated with spike height, but likely with spike duration. During both spontaneous and sensory-evoked fictive swimming, IPSCs and EPSCs in ENs increased. Although total inhibition far exceeded total excitation, firing rates were also increased, suggesting that the underlying excitatory and inhibitory synaptic input must be patterned during swimming to permit an elevation of cerebellar output.

## Materials and Methods

### Zebrafish

All procedures were performed on larval zebrafish 6-8 dpf according to National Institutes of Health guidelines and were approved by the Northwestern University Institutional Animal Care and Use Committee, protocols IS00000242 (I.M.R.) and IS00002671 (D.L.M.).

WT and transgenic zebrafish (*Danio rerio*) were kept in an in-house facility (Aquatic Habitats) in system water (28.5°C, pH 7.3, conductivity 550 $\mu$S) and maintained on a 14 h light:10 h dark cycle. Transgenic fish were kindly provided by the following investigators: *Tg[olig2:GFP]* fish, which express GFP in all olig2$^+$ cells, from Dr. Bruce Appel (University of Colorado, Denver) (McFarland et al., 2008); *Tg[Arch-tagRFP-T:car8:GCamp5]* fish ("Arch$^+$" fish), which express archaerhodopsin-3 in Purkinje cells, from Dr. Reinhard Köster (Technical University Braunschweig, Germany) (Matsui et al., 2014); and *Tg[vGlut2A:RG]* fish, which express dsRed in vGlut2$^+$ cells in the absence of Cre-recombinase, from Dr. Shin-ichi Higashijima (Okazaki Institute for Integrated Biology, Japan) (Miyashi et al., 2009). Crosses of these lines permitted combinatorial expression in larvae. Transgenic larvae were screened for green and/or red fluorescence at 5 dpf. Experiments were performed between 10:00 A.M. and 7:00 P.M. at room temperature (~22°C) on larval fish 6-8 dpf (before sexual differentiation).

*Electrophysiology*

Recordings were made as previously described (Harmon et al., 2017). Each larva was immobilized by immersion for 3 min in $\alpha$-bungarotoxin (1 mg/ml, Tocris Bioscience) in system water and then was transferred for 5 min to "extracellular solution" containing the following (in mM): 134 NaCl, 2.9 KCl, 2 $MgCl_2$, 10 HEPES, 10 glucose, and 2.1 $CaCl_2$, buffered to pH 7.8 with NaOH, with final osmolarity 290 mOsm. The immobilized fish was then placed in a Sylgard-lined plastic recording chamber containing extracellular solution plus MS-222 (0.01%) and pinned to the Sylgard with the dorsal side of the head and the left side of the tail facing upward. A midline incision was made, and the brain was exposed by pinning the skin. For recordings from peripheral motor nerves (i.e., ventral root), the skin was removed on the left side along the tail, from the rostral edge of the swim bladder to 3-5 segments rostral to the tip of the tail. The dissected preparation was then washed with several exchanges of MS-222-free extracellular solution before recordings were made.

The cerebellum was visualized on a FS2 Axioskop with IR-DIC (Carl Zeiss). Electrode positions and the locations of the rostral-lateral, rostral-medial, and caudal-medial edges of the corpus cerebellum were recorded from the coordinates of the MP-385 manipulator (Sutter Instrument). Relative positions of each cell were calculated using the distance between the electrode and each edge. For whole-cell recordings from ENs, borosilicate patch pipettes (8-12 M$\Omega$) were pulled on a P97 puller (Sutter Instrument) and filled with "intracellular solution" containing the following (in mM): 120 K-gluconate, 12 Na-gluconate, 3.2 NaCl, 2 $MgCl_2$, 0.025 $CaCl_2$, 1 EGTA, 0.3 Tris-GTP, 1 MgATP, 14 creatine phosphate, 10 HEPES, and 0.003 AlexaFluor-594 hydrazide, buffered to pH to 7.4 with KOH. Recordings from ENs in the left cerebellar hemisphere were made with a Multiclamp 700B and Digidata 1322A with pClamp software (Molecular Devices). Data were acquired at 20 kHz and filtered at 10 kHz. Command voltages were adjusted for the junction potential (−12 mV). Voltage-clamp recordings, compensated for capacitance but not series resistance, were made at corrected voltages of −75 mV ($E_{Cl}$) for EPSCs and 0 mV ($E_{cation}$) for IPSCs. In current-clamp, bridge balance and capacitance neutralization were applied.

For ventral root recordings, heat-polished patch pipettes (20-50 $\mu$m tip diameter) were bent to ~20° to optimize contact with the body wall. Pipettes filled with extracellular solution were positioned on the intermyotomal cleft at the 8-10 segment of the tail. Recordings were made with an Axopatch 200B amplifier (Molecular Devices) in current-clamp mode and bandpass filtered between 300 and 4000 Hz. Stimulus-evoked fictive swimming was elicited with a tactile stimulus consisting of a brief electrical current (1 mA, 5 ms) applied to the tail tip by a concentric bipolar stimulating electrode (WPI).

*Fluorescence, optogenetics, and electroporation*

ENs were identified by GFP fluorescence, elicited with a 488 nM blue LED (Thorlabs). Archaerhodopsin-3 (Arch) in Purkinje cells was activated by a 565 nM green LED (5400 lux; Thorlabs). Illumination was limited to the width of the cerebellum, and light application was gated with a Master-8 Pulse Stimulator (A.M.P.I.).

Pilot recordings from ENs in fish with Arch-expressing Purkinje cells revealed that IPSC rates were approximately half that of WT fish, suggesting that the GFP-activating light, which had been applied for several minutes to establish recordings, might have been sufficient to activate Arch and produce a lasting decrease in Purkinje cell simple spiking or that illumination otherwise influenced neuronal activity (Owen et al., 2019). Direct recordings from Purkinje cells exposed to 5 min of steady blue light ($N = 2$) confirmed a reduction in firing rates during illumination that recovered afterward only to 16% of the initial rate. This effect could be mitigated with strobed blue light (30 ms on and 30 ms off,

$N = 2$), after which firing returned to 41% of the initial rate. Therefore, the analysis of data from Arch$^+$ fish was limited to recordings from strobe-targeted neurons, and exposure of fish to high intensity light was kept to a minimum throughout the experiment. Arch activation was limited to 30-60 s, and no data were collected afterward. Within-cell comparisons were made of IPSCs before and during Arch activation. Because strobing facilitated visualization of GFP, this method was used in subsequent experiments for *Tg[olig2:GFP]* fish as well.

Single-cell electroporation was performed as described previously (Bhatt et al., 2007; Wang and McLean, 2014). Brains of MS-222-anesthetized *Tg[olig2:GFP]* fish were exposed as for electrophysiological recordings and placed in a chamber on the microscope stage. A glass recording pipette was filled with intracellular solution containing 0.3 $\mu$M AlexaFluor-594 (Invitrogen) and positioned with the tip contacting a GFP-labeled EN. Single current pulses (2-4 V for 1 ms) were applied while imaging the AlexaFluor-594 signal until dye was observed in the cell body, dendrite, and axon initial segment (usually within 1 min). A high-resolution $Z$ stack of filled neurons was collected with a 543 nm laser on a confocal microscope (Carl Zeiss LSM 710) with a 40×/1.0 NA water immersion objective (Carl Zeiss) and Zen imaging software and reconstructed in Imaris.

*Data analysis*

Electrophysiological data were analyzed in IGOR-Pro (Wavemetrics). Eurydendroid recordings were first smoothed with a 1 ms moving box average and then differentiated so that action potentials or synaptic currents could be identified by rate of rise (dV/dt or dI/dt). For current-clamp traces, action potentials were identified as events with a rate of rise $\geq$ 5 mV/ms. For voltage-clamp traces, the mean and SD were computed for all negative dI/dt values (to find EPSCs) and for all positive dI/dt values (to find IPSCs), and putative synaptic currents were identified as events exceeding 3 SDs from the mean. Events were discarded if they occurred <1 ms after the previous event. As a secondary check, the mean and SD of the currents (in the undifferentiated trace) associated with each dI/dt value were computed, and only EPSCs or IPSCs whose peak value was $\geq$2 SDs from the mean current were included in the analysis. Amplitudes of EPSCs and IPSCs were calculated relative to the baseline current averaged for 1 s preceding each event. Charge transfer was calculated for "isolated" EPSCs and IPSCs with no events for 10 ms before or after the event, zeroing the preceding baseline and integrating over 10 ms. Decay time constants of synaptic currents were estimated by single exponential fits to the mean of all isolated EPSCs or IPSCs from an individual cell. Cross-cell means were calculated from the average of the mean PSC amplitudes or mean change transfer of each cell. Swimming-related PSCs were classified as "summating" when the current deviated from baseline for >50 ms within 100 ms of the onset of a bout of swimming.

Ventral root recordings were rectified and smoothed with a 2 ms moving box average. The criterion for identification of a motor burst was a signal >5 SD above the mean noise in the smoothed record. A "bout" of fictive swimming was defined as a series of bursts with intervals of <100 ms. Instantaneous swimming frequency was calculated as the inverse of the interval between motor bursts. Firing rates associated with swimming were measured by calculating the instantaneous rate as the inverse of the interspike interval (ISI) and digitizing the rate at 1 kHz, and are reported as the mean over the first 200 ms of the swimming bout or as the peak of the firing rate averaged across all cells, as noted. Response latency was taken as the time at which firing exceeded 2 SDs above the baseline rate. To measure swimming-associated synaptic responses of ENs, current traces were aligned to bout onset, baseline zeroed, and averaged. Response latency was taken as the time to nonzero synaptic current for >50 ms in the averaged record, and response magnitude was taken as the mean current value for the average bout length of each recording.

To measure Purkinje cell spiking rate for estimating convergence estimates, data were reanalyzed from Harmon et al. (2017). A total of 27 recordings fulfilled the criteria of lasting >30 s before exposure to experimental stimuli and lacking spontaneous fictive swimming. Mean Purkinje cell firing rates, ISI distributions, peak membrane potential, and spike width were measured from spikes previously identified as simple or complex. Because the +dV/dt was maximal for simple spikes at a mean potential of −38 mV, spike widths for both simple and complex spikes were measured at this potential. Multipeaked spikes were identified as two or more positive-going zero-crossings in the differentiated record before the voltage fell below −38 mV. Predicted IPSC rates from converging Purkinje cells were estimated by randomly selecting 2 or 3 Purkinje cells and summing their mean firing rates.

*Statistical analysis*

$N$ values for biological replicates (cells, fish, and spikes) are reported in the text. Data are reported as mean ± SEM, except for Purkinje spike properties, which are reported as mean ± SD, as noted. Statistics were calculated with Microsoft Excel either with two-sided paired Student's $t$ tests (i.e., basally silent vs firing neurons; EPSCs vs IPSCs; IPSCs during vs before Arch activation; spiking or synaptic currents during spontaneous vs evoked swimming, or during swimming vs baseline), or with two-sided unpaired $t$ tests (i.e., IPSCs from Arch$^-$ vs Arch$^+$ fish), and $p$ values are reported.

## Results

### Anatomy and basal physiology of olig2$^+$ ENs

With a goal of studying how cerebellar output cells integrate inhibitory and excitatory input during fictive swimming in larval zebrafish, we began by labeling a population of ENs and characterizing their synaptic inputs. Previous work identified the transcription factor olig2 as a marker of calretinin-negative, non-Purkinje projection neurons in the intermediate cerebellum of the larval zebrafish, and classified these cells as ENs (McFarland et al., 2008; Bae et al., 2009; Matsui et al., 2014). Crossing fish that expressed RFP in Purkinje cells, *Tg[Arch-tagRFP-T:car8:GCamp5]* (Matsui et al., 2014) with *Tg[olig2:GFP]* fish permitted visualization of the relative position of olig2$^+$ cells and Purkinje neurons (Fig. 1*A*,*B*). Fluorescent olig2$^+$ cells were present throughout the corpus cerebelli, with some densely packed cells in the eminentia granularis (Fig. 1*B*). We counted 148, 194, and 232 olig2$^+$ neurons in the left hemisphere of 3 fish (7 dpf), indicating that the olig2$^+$ eurydendroid population is approximately the same size as the Purkinje cell population (Hamling et al., 2015). Electroporation of individual olig2$^+$ cells with AlexaFluor-594 ($N = 3$) revealed multiple dendritic branches extending into the molecular layer, as expected for ENs (Fig. 1*C*). Crossing *Tg[olig2:GFP]* fish with *Tg[vGlut2a:RG]* fish (Miyasaka et al., 2009) generated larvae in which the majority of olig2$^+$ cells in the cerebellum were also labeled with RFP, suggesting that most olig2$^+$ neurons are glutamatergic (Fig. 1*D*). The small number of olig2$^+$ cells that did not express vGlut2 may be olig2$^+$ oligodendrocytes, as reported in adult zebrafish (Bae et al., 2009). A subset of superficially located RFP$^+$ cells were not colabeled, indicating that not all glutamatergic cerebellar neurons express olig2. We took these observations, which are consistent with the description of olig2$^+$ ENs by McFarland et al. (2008), as a validation of the use of *Tg[olig2:GFP]* transgenic fish to identify ENs. All additional experiments were done on olig2$^+$ neurons, except as noted.

*Basal properties of spiking and synaptic inputs*

Whole-cell recordings were made in immobilized larval zebrafish 6-8 dpf from olig2$^+$ neurons across the rostrocaudal and mediolateral extent of the left cerebellar hemisphere (Fig. 2*A*,*B*). We previously found that fish at this developmental stage can engage in cerebellar dependent associative learning (Harmon et al., 2017), suggesting that the properties of ENs at this age, though likely immature, represent the activity of a functional cerebellar circuit. Current-clamp recordings demonstrated that most ENs

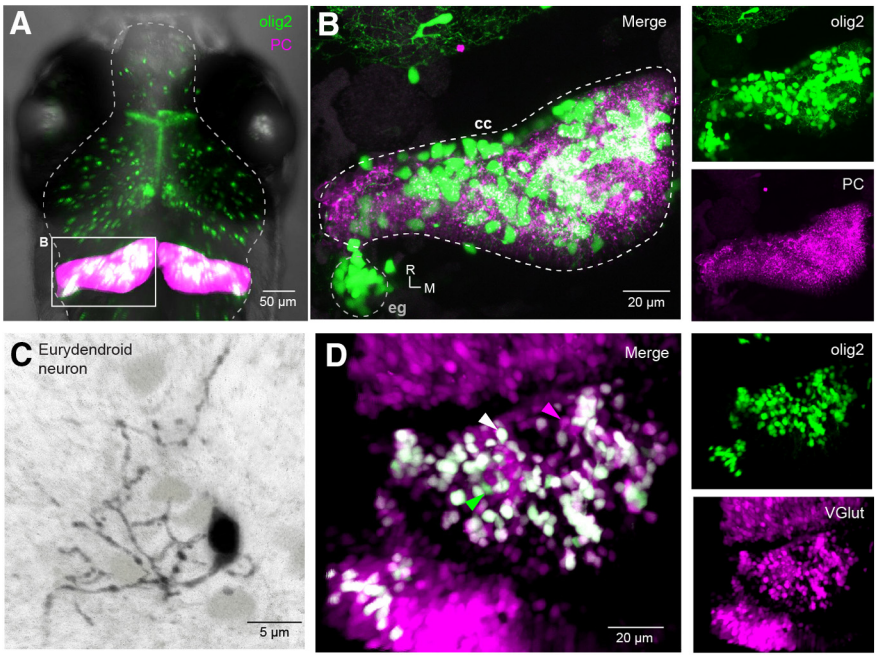


**Figure 1.** Identification of olig2$^+$ ENs in the zebrafish cerebellum. ***A***, Dorsal view of olig2$^+$ (green) and Purkinje (magenta) cells in the brain of a *Tg[olig2:GFP/Arch-tagRFP-T:car8:GCamp5]* fish (7 pdf). ***B***, Expansion of box in *A*, illustrating the left cerebellar hemisphere with olig2$^+$ eurydendroid (green) and Purkinje cells (magenta). cc, Corpus cerebelli; eg, eminentia granularis; R, rostral; M, medial. Insets, Right, Unmerged images of olig2$^+$ (top) and Purkinje (bottom) cells. ***C***, AlexaFluor-594-filled olig2$^+$ EN (black) with other GFP$^+$ ENs (light gray). ***D***, Dorsal view of the left cerebellar hemisphere in an *Tg[olig2:GFP/vGlut2a:RG]* fish. Arrows indicate cells that express both olig2 and vGlut2 (white), only olig2 (green), or only vGlut2 (magenta). Insets, Right, Unmerged images of green olig2$^+$ (top) and magenta vGlut2$^+$ cells (bottom).

($N = 16$ of 22) fired spontaneously (7.9 ± 1.5 spikes/s; Fig. 2*C*). The membrane potentials of basally silent cells were more depolarized than those of basally active cells during interspike periods (−34.3 ± 1.5 mV vs −39.3 ± 1.5 mV; $p = 0.04$), but silent cells were able to fire after applied hyperpolarizations (Fig. 2*C*, inset). Synaptic input, likely primarily from parallel fibers and Purkinje cells, was also evident in all neurons as EPSPs and IPSPs under current clamp or EPSCs and IPSCs under voltage clamp. Basally silent and firing cells had similar input resistances (2.4 ± 0.3 GΩ vs 2.5 ± 0.2 GΩ; $p = 0.9$), IPSC rates (12.1 ± 2.2 IPSCs/s vs 12.2 ± 4.3 IPSCs/s; $p = 0.96$), and EPSC rates (15.6 ± 3.7 EPSCs/s vs 19.1 ± 3.2 EPSCs/s; $p = 0.52$). Thus, as in the mammalian cerebellar nuclei, ENs tend to be intrinsically active and have a propensity for depolarization block that can be relieved by hyperpolarization (Jahnsen, 1986; Raman et al., 2000; Person and Raman, 2012a).

Next, we examined the properties of IPSCs measured at the cation reversal potential (0 mV). IPSCs had a 10%-90% rise time of 2.7 ± 0.2 ms and a maximal rate of rise of 20.9 ± 1.4 pA/ms ($N = 22$ cells, 22 fish; Fig. 2*D*). The single exponential decay time constant was 9.7 ± 0.6 ms (Fig. 2*D*, right), and the peak amplitude was 26.5 ± 1.5 pA (mode, 17 pA), giving a charge transfer of 182 ± 28 fC (mode, 90 fC; Fig. 2*F*,*G*). The interval between IPSCs was 84 ± 12 ms (mode, 5 ms; Fig. 2*H*). Since IPSCs, each with time constant of ~10 ms, occurred at intervals briefer than the basal ISI (~125 ms), Purkinje cells appear likely to exert a moderate tonic inhibitory control on eurydendroid cells.

Relative to IPSCs, EPSCs, measured at the Cl$^-$ reversal potential (−75 mV), had shorter rise times (10%–90%, 1.4 ± 0.3 ms, $N = 16$ cells, 16 fish; Fig. 2*E*) but a slower maximal rate of rise (−6.1 ± 0.53 pA/ms, $p < 0.001$); the faster rising rate of inhibition is consistent with the somatic location of Purkinje inputs (Alonso et al., 1992; Matsui et al., 2014). The single exponential decay time constant of EPSCs, however, was brief (1.9 ± 0.2 ms; Fig. 2*E*, right). The peak current magnitude and charge transfer were also smaller than for IPSCs, with means of −7.8 ± 1.8 pA and −23.5 ± 2.2 fC and modes near −3 pA and −15 fC ($p < 0.001$ for both values; Fig. 2*F*,*G*). Notably, at the mean membrane potential of all (silent and active) ENs of −38.3 ± 1.6 mV, the driving forces on IPSCs and EPSCs are approximately equal (~37 mV). Assuming perfusion by the extracellular solution of cerebellar tissue, which is relatively superficial, the conductance of individual inhibitory inputs is therefore threefold to fourfold larger than that of excitatory inputs. The mean interval between EPSCs was 65.8 ± 9.5 ms (15.2 ± 2.2 EPSCs/s), whereas the mode was near 4 ms (Fig. 2*H*).

### Estimating Purkinje-eurydendroid convergence

Next, we estimated the extent to which multiple Purkinje cells converge onto the same target EN. From previous recordings from Purkinje cells made under identical conditions, we reported that Purkinje cells generate simple spikes at 6.4 ± 1.2 spikes/s and complex spikes at 0.3 ± 0.03 spikes/s ($N = 27$) (Harmon et al., 2017). While the range of firing rates varied widely across cells (Fig. 3*A*, left), the coefficient of variation (CV) on the ISI was near 1 (1.24 ± 0.16; Fig. 3*B*,*C*, left). A CV near 1 can be taken as evidence that the ISIs have Poisson statistics (Tomko and Crapper 1974; Softky and Koch 1993). If different Purkinje cells fire independently, the intervals between IPSCs would also have a CV near 1; alternatively, if Purkinje cell firing is correlated, the CV should be increased, owing to distinct clusters of observations at high and at low intervals (Softky and Koch 1993). Although IPSC rates were variable across ENs (11.9 ± 1.7 IPSCs/s), the inter-IPSC interval distributions for each cell indeed had CVs near 1 (1.2 ± 0.06; Fig. 3*A*-*C*, right), consistent with convergence of independently firing Purkinje cells. Because mammalian Purkinje neurons, which spontaneously fire much more rapidly, have low ISI CVs (<0.1) (Häusser and Clark 1997; Raman and Bean 1999), we tested whether zebrafish Purkinje cells with

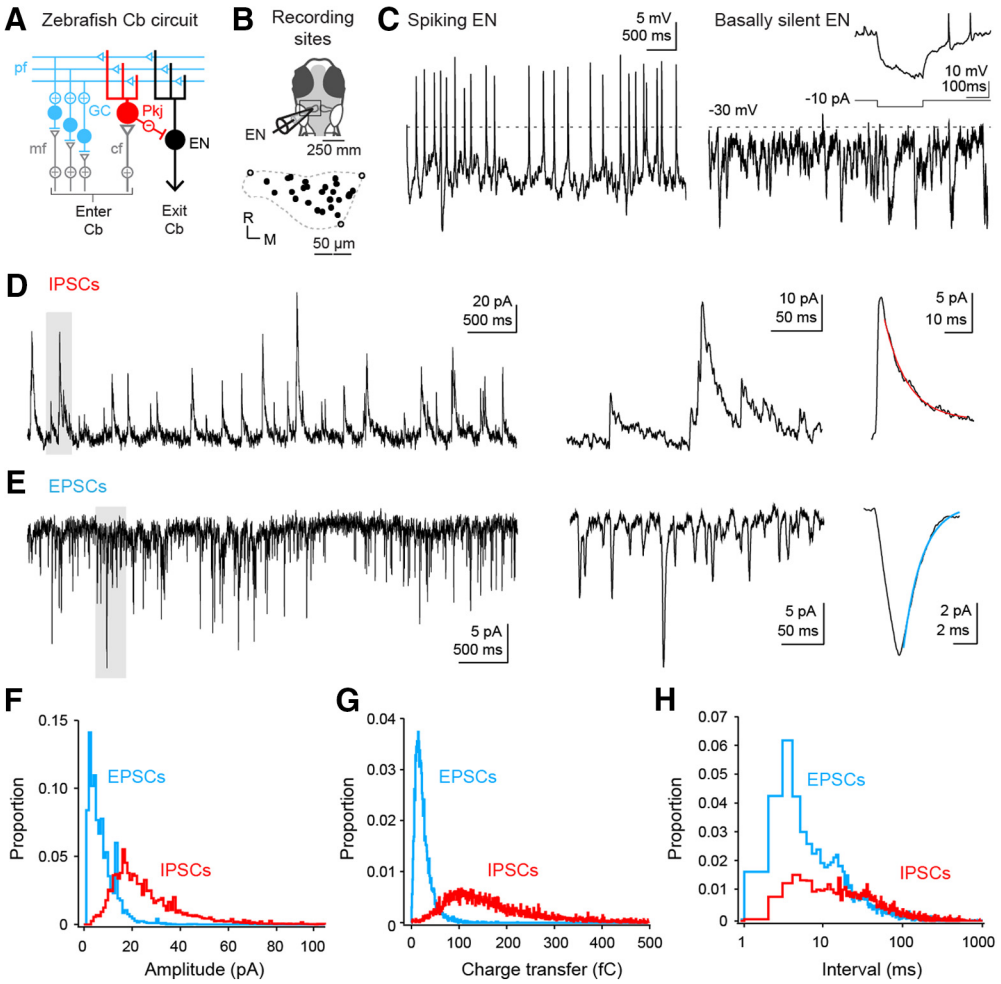


**Figure 2.** Basal firing, EPSCs, and IPSCs in ENs. ***A***, Simplified schematic of the zebrafish cerebellum. Cb, Cerebellum; mf, mossy fiber; pf, parallel fiber; cf, climbing fiber; GC, granule cell; Pkj, Purkinje cell. ***B***, Schematic of the recording configuration (top). Boxed region represents the left cerebellar hemisphere, expanded to show the positions of ENs from which recordings were made (bottom). R, Rostral; M, medial. Closed circles represent recording sites. Open circles represent position of rostral-lateral, rostral-medial, and caudal-medial edge. Dashed line indicates approximate dimensions of corpus cerebelli adapted from Figure 1*B*. ***C***, Current-clamp recordings from basally active (left) and basally silent (right) ENs. Dashed line indicates −30 mV. Scale bar applies to both traces. Inset, 200 ms hyperpolarizing current injection (−10 pA) into basally silent EN showing post-hyperpolarization spikes. ***D***, ***E***, Left, Voltage-clamp recording of spontaneous IPSCs (***D***) or EPSCs (***E***). Holding potential for IPSCs, 0 mV; EPSCs, −75 mV. Middle, Expansion of gray boxes at left. Right, Average of the average synaptic current of each cell in the dataset (EPSC, $N = 16$ cells; IPSC, $N = 22$ cells). Lines indicate single exponential fits (IPSC, $\tau = 9.7$ ms, red; EPSC, $\tau = 1.9$ ms, blue). ***F***, Probability histogram of the absolute amplitudes, relative to the preceding baseline, of all EPSCs (blue) and IPSCs (red). Bin width, 1 pA. ***G***, Probability histogram of absolute charge transfer of EPSCs (blue) and IPSCs (red) in the first 10 ms after the onset of the event. Bin width, 1 fC. ***H***, Probability histogram of inter-EPSC (blue) and inter-IPSC (red) intervals. Bin width, 1 ms.

higher basal rates fired more regularly. The interevent interval CV in each cell did not, however, correlate with either Purkinje firing rate or eurydendroid IPSC rate (Fig. 3*D*). Indeed, linear regression over the plots of CV against rate gave nearly flat lines (slope of 0.004 for Purkinje spikes and −0.01 for eurydendroid IPSCs) with intercepts near 1 (1.21 and 1.52, respectively), indicating Poisson statistics for all cells, regardless of firing or IPSC rate. Given these observations, the IPSC rates in ENs is expected to be the sum of the firing rates of converging Purkinje cells. Because the mean IPSC rate is close to double the mean Purkinje spike rate, the simplest analysis estimates that, on average, two Purkinje cells converge onto each EN.

The wide range of IPSC rates, however, suggests that not all ENs are contacted by exactly two Purkinje cells. We therefore estimated the range of convergence ratios by dividing the IPSC rate in each EN by the mean Purkinje firing rate of 6.7 spikes/s. This analysis predicted convergence ratios of 1 for the nine ENs with the lowest rates and as high as 5 for the single EN with the highest rate (31.8 IPSC/s; Fig. 3*E*). The high end of this is distribution is not well constrained, however, since Purkinje cell firing rate itself varies widely. To take this variance into consideration, we simulated IPSC histograms by randomly selecting 1, 2, or 3 Purkinje cells and summing their firing rates. These histograms encompassed the distribution of recorded IPSCs (Fig. 3*F*), with all IPSC rates falling within the sum of spike rates from 1 to 3 Purkinje cells. Together, these data indicate that most ENs receive inputs from 1 to 3 Purkinje afferents.

### Attributes of IPSCs from presynaptic simple and complex spikes

As seen in Figure 3*A*, intracellular recordings of spiking by larval zebrafish Purkinje cells show that climbing-fiber dependent "complex" spikes have twofold to fivefold larger amplitudes than simple spikes, likely because of large climbing-fiber EPSPs (Sengupta and Thirumalai, 2015; Harmon et al., 2017). This difference, coupled with the report that Purkinje axons can be very short (≤8 µm) in larval zebrafish (Matsui et al., 2014), raises the question of whether complex and simple spike-dependent

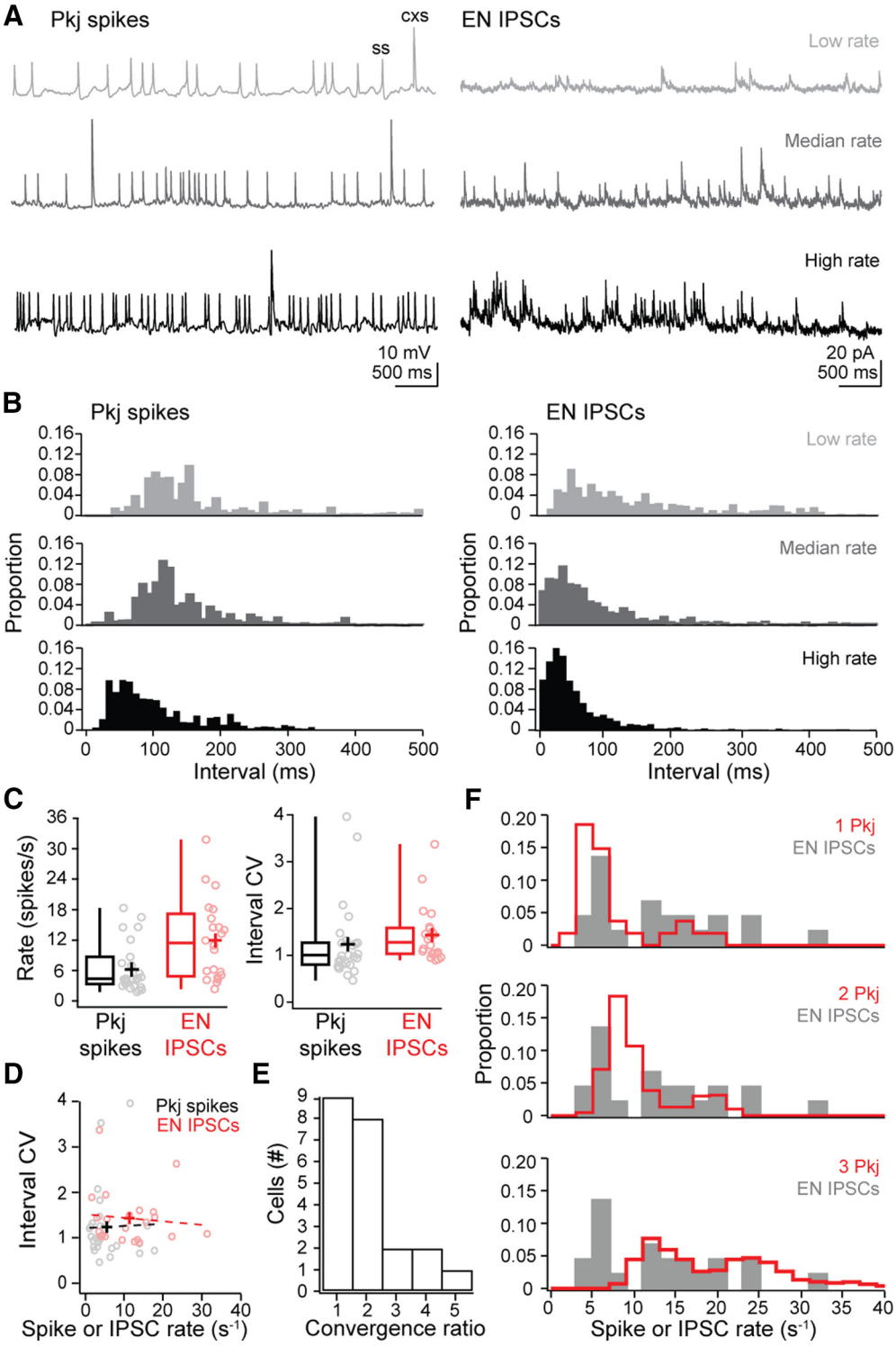


**Figure 3.** Estimates of Purkinje cell convergence onto ENs. ***A***, Example recordings of Purkinje cell (Pkj) spikes (left) and eurydendroid (EN) IPSCs (right), illustrating a low, median, and high rate (top, at the first quartile value; middle, median; bottom, third quartile value); ss, simple spike; cxs, complex spike. ***B***, Histograms of interevent intervals for Purkinje spikes (left) and IPSCs (right) from the recordings in *A*. Bin width, 10 ms. ***C***, Box-and-whisker plots of rate (left) and CV in the interevent interval (right) for Purkinje spikes (black) and eurydendroid IPSCs (red). Open circles represent data from individual cells. Crosses represent means. ***D***, Interval CV versus rate of Purkinje spikes (black) or eurydendroid IPSCs (red) for each cell. Dashed lines indicate linear fits to each distribution. ***E***, Histogram of the convergence ratios across cells estimated as the rounded ratio of IPSC rate to mean Purkinje cell spike rate. ***F***, Probability histogram of measured IPSC rates (gray) with the predicted distribution from 1, 2, or 3 Purkinje cells superimposed (red).

synaptic transmission is made equivalent by axonal filtering as in mammals (Khaliq and Raman 2005; Monsivais et al., 2005) or, alternatively, whether signals from the two types of Purkinje spikes generate distinct IPSCs in ENs. We therefore recorded from fish expressing Arch in Purkinje cells (Matsui et al., 2014; Harmon et al., 2017) to test whether IPSCs arising from presynaptic complex spikes had properties that distinguished them from other spontaneously occurring IPSCs.

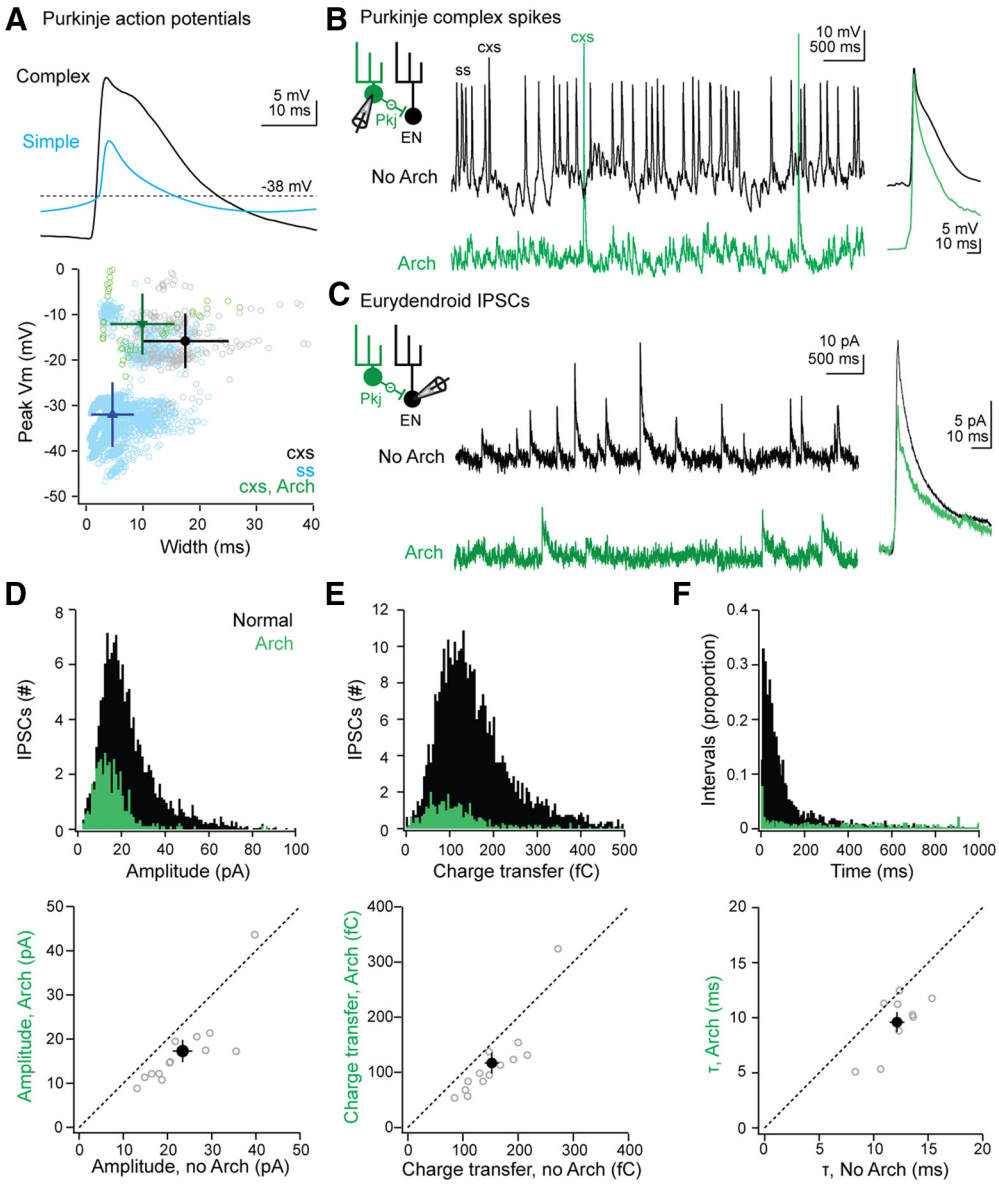


**Figure 4.** Properties of IPSCs resulting from Purkinje simple and complex spikes. ***A***, Top, Mean waveform of Purkinje cell simple (blue) and complex (black) spikes. Bottom, The peak spike voltage versus spike width for all events. All Purkinje cell recordings are from Harmon et al., 2017, and simple (blue) and complex (black) spikes were distinguished in that study based on conductance on the spike rising phase. Green represents complex spikes during Arch activation. Solid symbols represent mean ± SD. ***B***, Left, Schematic of recording setup. Pkj, Purkinje. Middle, Example current-clamp recordings without (black) and with (green) Arch activation. Right, Superimposed averaged complex spikes without and with Arch activation. ***C***, Left, Schematic of recording setup. Middle, Example voltage clamp recordings of spontaneous IPSCs in an EN without (black) and with (green) Arch activation. Right, Superimposed averaged IPSCs without and with Arch activation. ***D***, Top, Histogram of IPSC amplitude before (black) and during (green) Arch activation. Bin width, 1 pA. Bottom, Mean IPSC amplitude for each of 13 cells (open symbols) during versus before Arch activation. Solid symbol represents mean ± SEM. ***E***, Same as in ***D***, for charge transfer. Bin width, 1 fC. ***F***, Top, Same as in ***D***, for inter-IPSC intervals. Bin width, 1 ms. Bottom, Decay time constant of averaged IPSCs in each of 9 cells (open symbols) during versus before Arch activation. Solid symbol represents mean ± SEM.

We first examined the waveforms of Purkinje action potentials that we had recorded from WT fish in a previous study (Harmon et al., 2017). Spikes had been classified as simple or complex based on their rate of rise ($N = 4199$ simple spikes and 208 complex spikes from 27 Purkinje cells; to convey the breadth of the distribution, the SD rather than SEM is given for spike attributes). Complex spikes reached a peak voltage of $-15.8 \pm 6.0$ mV, and 63.3% ($N = 131$ of 208) had more than one peak, generating a spike width at −38 mV of 17.4 ± 7.6 ms (Fig. 4*A*, black). Most simple spikes were smaller, with a peak voltage of $-32.0 \pm 7.1$ mV, and 93% ($N = 3926$ of 4199) had only one peak, yielding a narrower spike width of 4.7 ± 3.8 ms (Fig. 4*A*, blue). The remaining spikes with rise times typical of simple spikes (7%) included a shoulder or a second peak, reached a voltage of $-19.2 \pm 9.7$ mV, and had spike widths of 15.7 ± 5.0 ms. These events may be simple spikes with a Ca-dependent hump (Sengupta and Thirumalai, 2015) or simple spikes followed rapidly by a climbing-fiber EPSP. Although their classification remains ambiguous, they represent a small fraction of simple spikes.

Next, we compared these observations to the waveforms of spikes recorded in Arch-expressing Purkinje cells. We previously found that Arch activation hyperpolarizes the membrane potential by 25-30 mV, greatly reducing the simple spike rate without changing the complex spike rate (Harmon et al., 2017).

Comparing the complex spikes elicited without and with Arch activation (Fig. 4*A*, bottom, *B*) showed that these events had indistinguishable peak voltages (without vs with Arch, −12.1 ± 2.9 mV vs −12.4 ± 2.2 mV; $N = 43$ vs 53 spikes in 7 cells, $p = 0.94$). Complex spikes, however, were briefer during Arch activation (without vs with Arch, 28.8 ± 4.8 ms vs 10.7 ± 3.0 ms; $p = 0.007$; Fig. 4*B*), and only 27.3% were multipeaked. Thus, IPSCs recorded in ENs during presynaptic Arch-induced hyperpolarization are expected to result predominantly from complex spikes with normal peak amplitudes but briefer durations.

With this information in hand, we recorded from identified ENs while suppressing Purkinje simple spikes through Arch activation in compound *Tg[olig2:GFP; Arch-tagRFP-T:car8:GCamp5]* larvae, and measured IPSCs with and without optical stimulation in the same set of ENs ($N = 13$ cells). Consistent with a dominant contribution of Purkinje cell simple spikes to the generation of eurydendroid IPSCs, Arch activation decreased IPSC rates approximately fivefold, from 6.6 ± 1.7 to 1.4 ± 0.3 IPSCs/s ($p = 0.006$; Fig. 4*C*,*D*, top). Before Arch activation, IPSCs had a mean amplitude of 23.4 ± 2.2 pA and charge transfer of 152 ± 13 fC (Fig. 4*D*, *E*; $p > 0.2$ vs control recordings from Arch-lacking fish). During Arch activation, the mean became smaller, with an amplitude of 17.3 ± 2.5 pA ($p < 0.001$) and charge transfer of 117 ± 19 fC ($p = 0.009$; Fig. 4*D*,*E*). To test whether the decreased charge transfer was simply a consequence of the reduced amplitude or also reflected an effect on kinetics, we measured the time constant of decay from neurons in which the mean IPSC was >10 pA ($N = 9$ cells). Arch activation decreased the decay constant as well, from 12.1 ± 0.7 to 9.6 ± 0.9 ms ($p = 0.004$; Fig. 4*F*). Comparing the interval distributions for IPSCs showed that the skewed Gaussian present in control conditions was flatter during simple spike suppression. Only 1 of 13 cells showed IPSCs at brief intervals (Fig. 4*F*), suggesting that the clusters of IPSCs with shorter intervals under control conditions are likely due to simple rather than complex spikes.

Together, these data demonstrate that the amplitude of IPSCs in eurydendroid cells is not determined solely by the height of the presynaptic Purkinje action potential. Specifically, although the amplitudes of the complex spikes are preserved during Arch activation, the distribution of IPSCs during Arch activation was not skewed toward large events, nor were small events preferentially lost. On the contrary, the mean IPSC amplitude and charge transfer were reduced by ~25%. These remaining IPSCs were likely evoked primarily by high-amplitude but narrow presynaptic complex spikes. The results therefore suggest that the longer duration of normal complex spikes, and possibly of simple spikes with Ca-dependent shoulders, may prolong and amplify IPSCs.

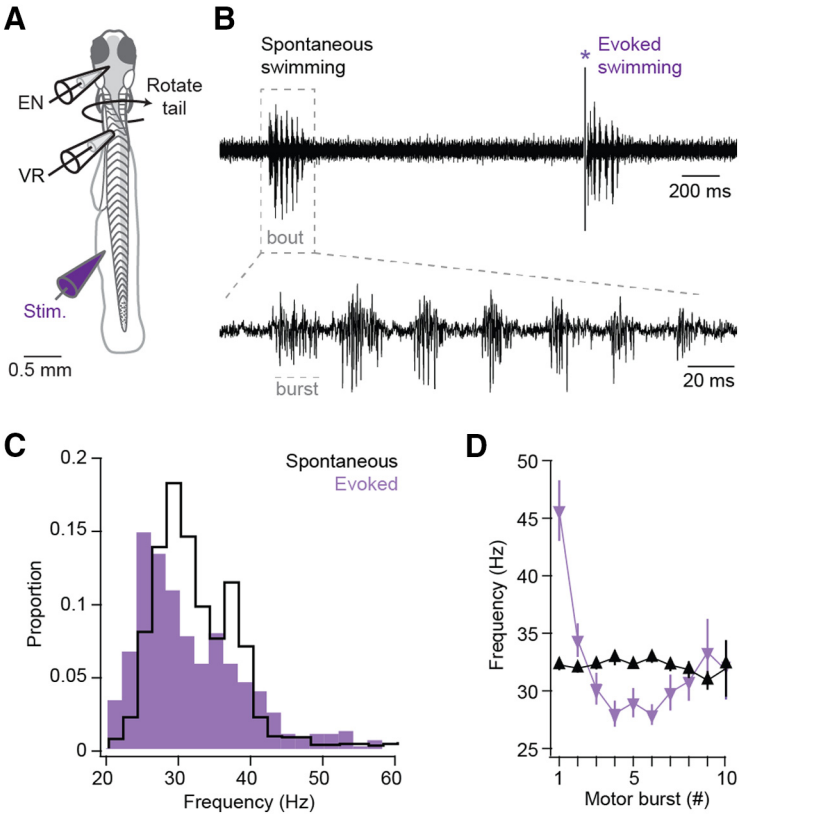


**Figure 5.** Comparison of ventral root (VR) activity during spontaneous and sensory-evoked fictive swimming. ***A***, Diagram of preparation during simultaneous EN and VR recordings. ***B***, Top, Example VR recording of bouts of spontaneous (left) and evoked (right) fictive swimming. *Stimulus artifact. Dashed box represents segment of trace expanded at bottom to illustrate bursts within the bout, as labeled. Dashed line indicates a motor burst. ***C***, Probability histogram of burst frequency during evoked (purple) and spontaneous (black) swimming. Bin width, 1 Hz. ***D***, Mean burst frequency for the first 10 bursts for bouts of evoked (purple) and spontaneous (black) swimming.

## Spiking and synaptic responses during spontaneous and evoked swimming

We previously found that conditioned fictive swimming in larval zebrafish depends on changes in Purkinje cell activity (Harmon et al., 2017), raising the possibility that the activity of the ENs has the capacity to influence locomotion. Therefore, we next recorded from neurons while simultaneously monitoring fictive swimming with ventral root recordings (Fig. 5*A*). Bouts of swimming consisted of cyclical motor bursts that normally drive rhythmic tail movements, and swimming either occurred spontaneously or was evoked with a brief tactile stimulus to the tail (Fig. 5*B*). Spontaneous swimming bouts lasted 269 ± 21 ms and were composed of 10.0 ± 2.0 bursts at 31.9 ± 1.0 Hz (Fig. 5*C*). Evoked swimming bouts occurred with a latency of 21.3 ± 2.1 ms from the stimulus, lasted 256 ± 42 ms and consisted of 8.4 ± 1.7 motor bursts at 33.1 ± 1.6 Hz (Fig. 5*C*). Ventral root motor burst frequency remained relatively uniform during spontaneous bouts but started high and decreased over the course of evoked bouts (Fig. 5*D*).

During fictive swimming, almost all current-clamped ENs increased their firing rates (Fig. 6*A*,*B*). Firing during spontaneous swimming was elevated in 10 of 11 cells, from a baseline of 11.1 ± 1.3 to 20.2 ± 3.4 spikes/s averaged over the first 200 ms of swimming ($p = 0.01$). Similarly, 8 of 9 cells increased their firing rates during evoked swimming, from 8.2 ± 1.7 spikes/s to 17.9 ± 3.7 spikes/s, also averaged over 200 ms ($p = 0.016$). For spontaneous swimming, the instantaneous firing rate surpassed 2 SDs above baseline 21 ms after bout onset, peaked after 37 ms

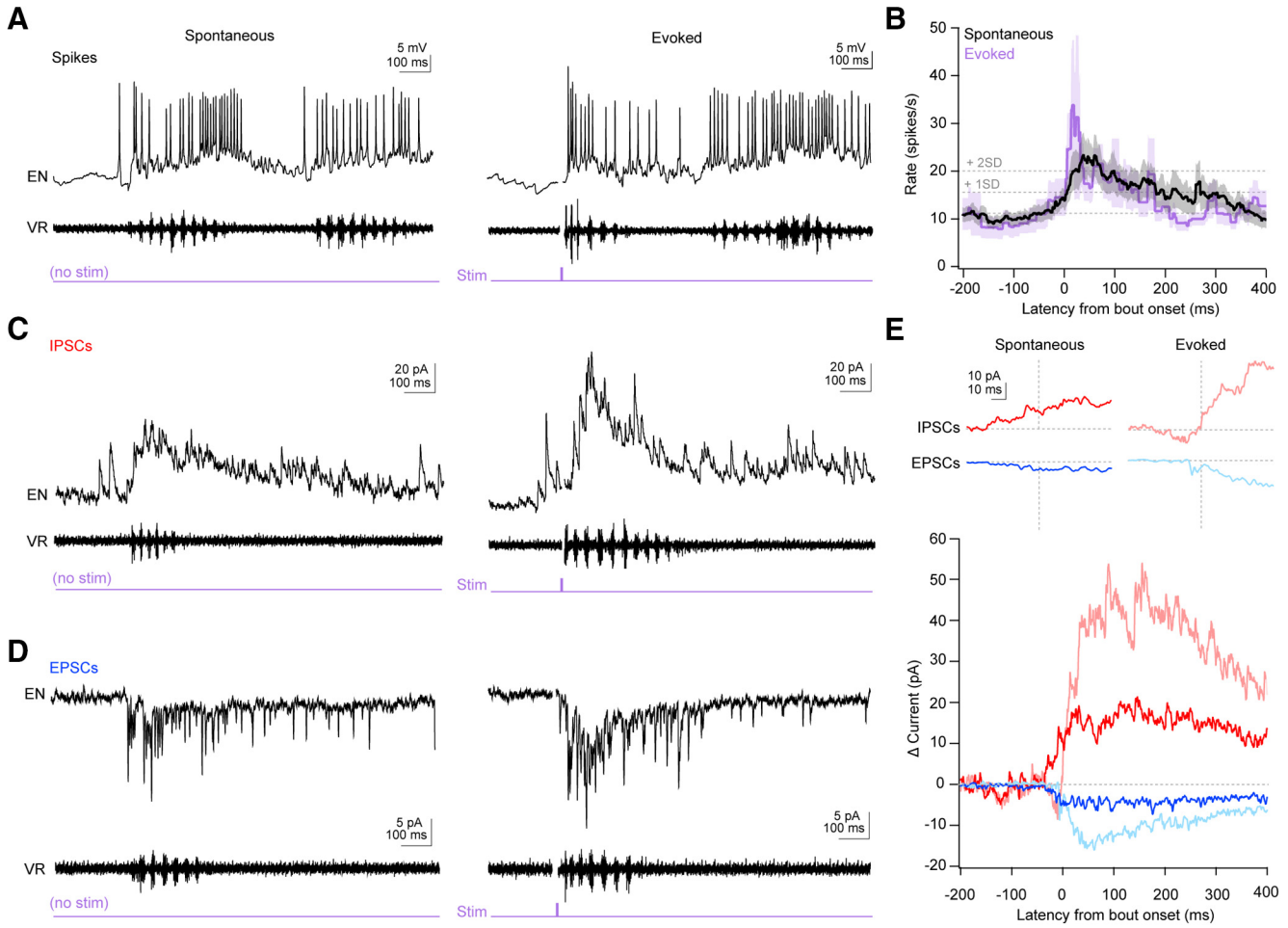


**Figure 6.** Action potential firing and synaptic responses of ENs during spontaneous and sensory-evoked swimming. ***A***, Example records of spikes from a single current-clamped EN (top), ventral root recording (middle), and time of 5 ms tactile stimulus to the tail (bottom), for spontaneous (left) and evoked (right) swimming. Stimulus artifact is blanked. ***B***, Mean ± SEM instantaneous spike rate during spontaneous (black) and evoked (purple) swimming, digitized at 1 kHz. Dotted lines indicate mean basal firing rate plus 1 or 2 SDs. IPSCs (***C***) or EPSCs (***D***) from a single cell with ventral root recordings during spontaneous (left) and evoked (right) swimming. ***E***, Top, High gain illustration of onset of responses shown below. Vertical dotted line indicates swimming onset. Horizontal dotted lines indicate zero current. All plots are on the same scale. Bottom, Mean inhibitory (red) and excitatory (blue) currents during evoked (light lines) and spontaneous (dark lines) swimming. Time zero indicates bout onset. Recordings were zeroed to the mean holding current 1 s before bout onset and averaged across all bouts for each cell.

(24.1 ± 5.1 spikes/s), and remained elevated for 75 ms. For evoked swimming, the instantaneous firing rate exceeded 2 SDs above baseline only 6 ms after bout onset, reached a peak of 33.8 ± 13.6 spikes/s at 17 ms, then fell back toward baseline at 40 ms. Thus, ENs show swimming-associated firing, but spontaneous and stimulus-evoked swimming was associated with responses with different magnitudes and time courses. Firing rates of individual cells did not appear to be consistently modulated with specific phases of the motor burst cycle, although the limited number of spikes precluded a detailed analysis. These results are consistent with the idea that, as in mammals, cerebellar output occurs in association with locomotor behavior and may influence and/or report movements.

To examine the synaptic input underlying the changes in firing, we made voltage-clamp recordings of Purkinje-mediated IPSCs (spontaneous: 70 bouts, 17 fish; evoked: 16 bouts, 14 fish; Fig. 6*C*) and parallel fiber-mediated EPSCs (spontaneous: 89 bouts, 14 fish; evoked: 18 bouts, 18 fish; Fig. 6*D*) associated with fictive swimming. During swimming, synaptic currents often occurred at high frequencies such that they summated and individual events could not be distinguished. Therefore, the inhibitory currents at 0 mV or excitatory currents at −75 mV were aligned to the onset of each bout of swimming, baseline subtracted, and averaged within each cell, and the mean of all the averages was plotted (Fig. 6*E*). This analysis demonstrated that both IPSCs and EPSCs increased in association with spontaneous as well as evoked swimming, but the magnitude and timing of synaptic input differed between types of swimming.

To quantify these differences, we measured the latency to the onset of summation of PSCs as well as the magnitude of the mean synaptic current over the duration of the bout. Comparisons were limited to recordings of IPSCs or EPSCs made from cells in which we had recorded both kinds of swimming ($N = 12$). For spontaneous bouts, IPSCs began to increase before swimming, with a latency of −25.1 ± 11.3 ms (Fig. 6*E*, dark red). For evoked bouts, swimming began 10-50 ms after the electrical stimulation of the tail (Harmon et al., 2017); as a result, blanking of the stimulus artifact precluded quantitative measurement of PSC amplitudes in this window. Inspection of individual records, however, indicated that the increase in IPSCs indeed lagged swimming, with a latency of 28.1 ± 10.2 ms (Fig. 6*E*, light red, $p = 0.004$). The mean inhibitory current over the full bout duration was twice as large for evoked relative to spontaneous swimming (31.8 ± 7.0 pA vs 15.8 ± 3.5 pA; $p = 0.016$).

Similarly, EPSCs began to summate before spontaneous swimming but after evoked swimming (lags, $-16.9 \pm 9.8$ ms and $8.2 \pm 3.7$ ms, Fig. 6*E*, dark blue vs light blue; $p = 0.06$). The mean excitatory current was nearly triple for evoked versus spontaneous swimming ($8.4 \pm 1.8$ pA vs $2.9 \pm 0.7$ pA; $p = 0.009$). Thus, within-cell comparisons illustrated that the total synaptic input was much greater for evoked than for spontaneous swimming. Additionally, the total inhibition far exceeded excitation during both kinds of swimming (Fig. 6*E*, spontaneous, $p = 0.002$; evoked, $p = 0.02$). The observation that ENs increase their firing rates during both kinds of bouts indicates that they respond with spiking to swimming-associated elevations of excitation despite the predominance of inhibitory input.

## Discussion

These results demonstrate that olig2$^+$ ENs in the cerebellum of larval zebrafish, like their homologs in the mammalian CbN, tend to be intrinsically active. Each EN is inhibited by 1-3 functional Purkinje cells. Optogenetic manipulation of Purkinje cells suggests that IPSCs from complex and simple spikes are not obviously distinct, but that broader presynaptic action potentials, most often associated with complex spikes, may elicit stronger inhibition of ENs. During fictive swimming, synaptic excitation and inhibition both increase. The total inhibition far exceeds excitation, yet firing rates of ENs increase, indicating that parallel fibers drive spikes effectively despite elevated input from Purkinje cells. Together, the data demonstrate that olig2$^+$ ENs integrate Purkinje and parallel fiber inputs in a manner that elevates cerebellar output during locomotion.

### Olig2$^+$ neurons as cerebellar output neurons

Cerebellar neurons expressing the transcription factor olig2 in larval zebrafish label a subset of calretinin-negative cells that are likely to be ENs, based on their morphology, location, and distinction from Purkinje cells (McFarland et al., 2008). Studies of adult fish confirm that, although a minority of olig2$^+$ cells are oligodendrocytes, most are neurons that express vGlut2 and project to known cerebellar targets (McFarland et al., 2008; Heap et al., 2013). Also, Purkinje cell axons terminate on their cell bodies, providing further evidence that many olig2$^+$ cells are indeed ENs that transmit cerebellar output (Alonso et al., 1992; Bae et al., 2009; Matsui et al., 2014).

The present experiments, which provide electrophysiological *in vivo* data from olig2$^+$ neurons, confirm the following: (1) olig2$^+$ cells of ~7 dpf larval zebrafish produce action potentials either spontaneously or after hyperpolarizing current injections; (2) they generate EPSCs and IPSCs, which both increase with fictive swimming; and (3) they receive inhibition that is reduced by optogenetically suppressing Purkinje simple spikes. Together, these observations provide physiological evidence not only that olig2$^+$ cells are indeed ENs but also that they are functional targets of Purkinje cells already at the larval stage. As such, they appear likely to carry cerebellar signals that may influence or report volitional and learned movements (Aizenberg and Schuman 2011; Ahrens et al., 2012; Sengupta and Thirumalai, 2015; Scalise et al., 2016; Harmon et al., 2017).

### Eurydendroid cell activity during motor behavior

During spontaneous and sensory-evoked fictive swimming, EN spiking and synaptic currents both increase. The increase in cerebellar output may reflect a cerebellar contribution to locomotion, as in mammals (Orlovsky, 1972; Armstrong and Edgley 1984; Sarnaik and Raman 2018), and/or a sensorimotor signal that relays sensory expectations, reports motor commands, and/or primes fish for subsequent learning (Knogler et al., 2019). Interestingly, however, although firing rates and synaptic drive increased during swimming, the total inhibitory conductance far outweighed the excitatory conductance.

Multiple factors may contribute to these observations. First, excitation may consistently precede inhibition. ENs are inhibited by Purkinje cells, and, unlike their mammalian homologs, are excited directly by parallel fibers (Meek et al., 1992; Han and Bell, 2003; Bae et al., 2009). Therefore, if parallel fibers contact connected Purkinje and ENs, excitation may permit eurydendroid firing before feedforward inhibition arrives. Second, since ENs resting at depolarized potentials in the basal state could fire on termination of hyperpolarizing current injections, a propensity for depolarization block, as in mouse CbN cells (Raman et al., 2000), may lead Purkinje-mediated inhibition to facilitate firing by permitting voltage-gated Na channels to recover from inactivation.

### Convergence of Purkinje cells onto ENs

A question in cerebellar processing is the extent of divergence and convergence of Purkinje axons. In many vertebrates, Purkinje cells outnumber cerebellar output neurons; the Purkinje to CbN cell ratio is ~30:1 in cats and ~10:1 in mice (Palkovits et al., 1977; Caddy and Biscoe 1979). Based on evidence that parvalbumin is a marker for Purkinje cells (Bae et al., 2009; Takeuchi et al., 2017), counts of parvalbumin-positive neurons estimate 250–300 Purkinje cells in the cerebella of 6–7 dpf zebrafish larvae (Hamling et al., 2015). Doubling the single-hemisphere counts made here of olig2$^+$ cells estimates 300–400 such cells at 7 dpf. Since oligodendrocytes account for a minor but non-zero fraction of olig2$^+$ cells in adult zebrafish (Bae et al., 2009), this value likely slightly overestimates the number of olig2$^+$ Purkinje target neurons. These cell counts therefore suggest that the ratio of Purkinje to olig2$^+$ ENs may be near 1:1 at ~7 dpf. The existence of calretinin-positive, olig2-negative ENs, however (Bae et al., 2009), raises the possibility that cerebellar output neurons outnumber Purkinje cells in larval zebrafish.

In many vertebrates, however, Purkinje cells diverge to contact multiple targets (Chan-Palay, 1977; Palkovits et al., 1977; De Zeeuw et al., 1994; Wylie et al., 1994; Teune et al., 1998; Sugihara et al., 2009). Consequently, convergence cannot be estimated from a simple ratio of cell counts. In mice, Purkinje axons ramify greatly (Palkovits et al., 1977), and tens of Purkinje cells apparently contact an individual CbN cell (Person and Raman 2012a, b). In zebrafish larvae, however, the visualization of Purkinje cell morphology with wheat-germ-agglutinin expression indicates that axons extend for $<8$ μm, with a mean length near 2 μm (Matsui et al., 2014). With such short axons, extensive divergence seems unlikely.

Nevertheless, we find that the mean rate of spontaneous IPSCs in ENs (~12 events/s) is about twice than predicted from basal firing rates of Purkinje cells (~6 spikes/s). Since Purkinje cells appear to be the primary source of inhibition to ENs, this observation suggests that Purkinje cell convergence occurs despite short axons. Accounting for variation in Purkinje spiking and eurydendroid IPSCs suggested that most target neurons receive 1-3 Purkinje inputs. If Purkinje action potentials do not always elicit a measurable IPSC, or if some afferent Purkinje cells were silent under the conditions of the recordings, then the

anatomic convergence may be greater than we estimated functionally.

### Responses to different types of Purkinje spikes

The short Purkinje axons also raise the possibility that the extreme differences in simple and complex spike waveforms evident in larval zebrafish Purkinje somata (Hsieh et al., 2014; Sengupta and Thirumalai 2015; Scalise et al., 2016; Harmon et al., 2017) might lead to differences in magnitudes or durations of neurotransmitter release. In rodents, each complex spike elicits 2-3 axonal action potentials because of spikelets riding on giant synaptic potentials (Khaliq and Raman, 2005; Monsivais et al., 2005); although in larval zebrafish complex spikes do not always show discrete spikelets, most have second peaks or a shoulder on the falling phase (Sengupta and Thirumalai, 2015; Harmon et al., 2017). Optogenetically hyperpolarizing Purkinje cells to reduce simple spiking decreased IPSC rates approximately fivefold, demonstrating that the majority of inhibition to olig2$^+$ ENs originates from Purkinje simple spikes. Although the residual complex spikes during Arch activation retained high amplitudes, IPSCs were smaller than in control conditions. Complex spikes during Arch activation, however, were narrowed and lacked secondary peaks, suggesting that the normally broad complex spike may facilitate transmitter release by permitting multiple axonal spikes (Khaliq and Raman 2005; Monsivais et al., 2005) or prolonged depolarization of the synaptic terminal (Geiger and Jonas, 2000).

### Eurydendroid signaling during movement and learning

Fictive swimming can occur in larval zebrafish, even after cerebellar ablation, indicating that the cerebellum is not absolutely required for locomotion. The cerebellum is required for associative learning of swimming in response to sensory input, however, suggesting that it must influence brain regions that drive locomotion (Harmon et al., 2017). During learning, Purkinje cells alter their firing and can be classified based on whether they begin generating sensory-associated complex spikes, motor-associated complex spikes, or sensory-associated simple spikes. These response groups are segregated topologically, consistent with reports of organization of the zebrafish cerebellum along the mediolateral axis (Heap et al., 2013; Matsui et al., 2014; Knogler et al., 2019). The IPSCs in the present study, which sampled ENs across the cerebellar hemisphere, suggest that complex as well as simple spikes are transmitted downstream, and learning-related alterations in both types of spikes may directly influence cerebellar output.

In general, however, the firing rate of ENs was elevated, rather than suppressed, with spontaneous and evoked swimming. It therefore seems likely that ENs may change their activity as fish learn to swim in response to arbitrary stimuli. The previous observation that Purkinje simple spikes are necessary for acquisition and expression of early conditional swimming responses, but not for expression of well-learned conditional responses (Harmon et al., 2017), suggests that learning-associated plasticity likely takes place at synapses onto ENs, as in the mammalian CbN (García and Mauk 1998; Medina and Mauk 1999; Pugh and Raman 2006, 2008; McElvain et al., 2010; Person and Raman 2010).

## References


Ahrens MB, Li JM, Orger MB, Robson DN, Schier AF, Engert F, Portugues R (2012) Brain-wide neuronal dynamics during motor adaptation in zebrafish. Nature 485:471–477.

Aizenberg M, Schuman EM (2011) Cerebellar-dependent learning in larval zebrafish. J Neurosci 31:8708–8712.

Alonso JR, Arevalo R, Briñon JG, Lara J, Weruaga E, Aijon J (1992) Parvalbumin immunoreactive neurons and fibres in the teleost cerebellum. Anat Embryol 185:355–361.

Armstrong DM, Edgley SA (1984) Discharges of nucleus interpositus neurones during locomotion in the cat. J Physiol 351:411–432.

Bae YK, Kani S, Shimizu T, Tanabe K, Nojima H, Kimura Y, Higashijima S, Hibi M (2009) Anatomy of zebrafish cerebellum and screen for mutations affecting its development. Dev Biol 330:406–426.

Bhatt DH, McLean DL, Hale ME, Fetcho JR (2007) Grading movement strength by changes in firing intensity versus recruitment of spinal interneurons. Neuron 53:91–102.

Brown ST, Raman IM (2018) Sensorimotor integration and amplification of reflexive whisking by well-timed spiking in the cerebellar corticonuclear circuit. Neuron 99:564–575.e2.

Caddy KW, Biscoe TJ (1979) Structural and quantitative studies on the normal C3H and Lurcher mutant mouse. Philos Trans R Soc Lond B Biol Sci 287:167–201.

Castro A, Becerra M, Manso MJ, Anadón MJ (2006) Calretinin immunoreactivity in the brain of the zebrafish, *Danio rerio*: distribution and comparison with some neuropeptides and neurotransmitter-synthesizing enzymes: II. Midbrain, hindbrain, and rostral spinal cord. J Comp Neurol 494:792–814.

Chan-Palay V (1977) Cerebellar dentate nucleus: organization, cytology and transmitters. Berlin: Spring-Verlag.

Chen S, Augustine GJ, Chadderton P (2016) The cerebellum linearly encodes whisker position during voluntary movement. eLife 5:e10509.

De Zeeuw CI, Wylie DR, DiGiorgi PL, Simpson JI (1994) Projections of individual Purkinje cells of identified zones in the flocculus to the vestibular and cerebellar nuclei in the rabbit. J Comp Neurol 349:428–447.

García KS, Mauk MD (1998) Pharmacological analysis of cerebellar contributions to the timing and expression of conditioned eyelid responses. Neuropharmacology 37:471–480.

Geiger JR, Jonas P (2000) Dynamic control of presynaptic $Ca^{2+}$ inflow by fast-inactivating $K^+$ channels in hippocampal mossy fiber boutons. Neuron 28:927–939.

Goodkin HP, Thach WT (2003) Cerebellar control of constrained and unconstrained movements: I. Nuclear inactivation. J Neurophysiol 89:884–895.

Hamling KR, Tobias ZJ, Weissman TA (2015) Mapping the development of cerebellar Purkinje cells in zebrafish. Dev Neurobiol 75:1174–1188.

Han VZ, Bell CC (2003) Physiology of cells in the central lobes of the mormyrid cerebellum. J Neurosci 23:11147–11157.

Harmon TC, Magaram U, McLean DL, Raman IM (2017) Distinct responses of Purkinje neurons and roles of simple spikes during associative motor learning in larval zebrafish. eLife 6:e22537.

Häusser M, Clark BA (1997) Tonic synaptic inhibition modulates neuronal output pattern and spatiotemporal synaptic integration. Neuron 19:665–678.

Heap LA, Goh CC, Kassahn KS, Scott EK (2013) Cerebellar output in zebrafish: an analysis of spatial patterns and topography in eurydendroid cell projections. Front Neural Circuits 7:53.

Heiney SA, Kim J, Augustine GJ, Medina JF (2014) Precise control of movement kinematics by optogenetic inhibition of Purkinje cell activity. J Neurosci 34:2321–2330.

Hsieh J, Ulrich B, Iss FA, Wan J, Papazian DM (2014) Rapid development of Purkinje cell excitability, functional cerebellar circuit, and afferent sensory input to cerebellum in zebrafish. Frontiers of Neural Circuits 8:147.

Jahnsen H (1986) Electrophysiological characteristics of neurones in the guinea-pig deep cerebellar nuclei in vitro. J Physiol 372:129–147.

Khaliq ZM, Raman IM (2005) Axonal propagation of simple and complex spikes in cerebellar Purkinje neurons. J Neurosci 25:454–463.

Knogler LD, Kist AM, Portugues R (2019) Motor context dominates output from Purkinje cell functional regions during reflexive visuomotor behaviours. eLife 8:e42138.

Lee KH, Mathews PJ, Reeves AM, Choe KY, Jami SA, Serrano RE, Otis TS (2015) Circuit mechanisms underlying motor memory formation in the cerebellum. Neuron 86:529–540.

Matsuda K, Yoshida M, Kawakami K, Hibi M, Shimizu T (2017) Granule cells control recovery from classical conditioned fear responses in the zebrafish cerebellum. Sci Rep 7:11865.

Matsui H, Namikawa K, Babaryka A, Koster RW (2014) Functional regionalization of the teleost cerebellum analyzed in vivo. Proc Natl Acad Sci USA 111:11846–11851.

McCormick DA, Thompson RF (1984) Neuronal responses of the rabbit cerebellum during acquisition and performance of a classically conditioned nictitating membrane-eyelid response. J Neurosci 4:2811–2822.

McElvain LE, Bagnall MW, Sakatos A, du Lac S (2010) Bidirectional plasticity gated by hyperpolarization controls the gain of postsynaptic firing responses at central vestibular nerve synapses. Neuron 68:763–775.

McFarland KA, Topczewska JM, Weidinger G, Dorsky RI, Appel B (2008) Hh and Wnt signaling regulate formation of olig2$^{+}$ neurons in the zebrafish cerebellum. Dev Biol 318:162–171.

Medina JF, Mauk MD (1999) Simulations of cerebellar motor learning: computational analysis of plasticity at the mossy fiber to deep nucleus synapse. J Neurosci 19:7140–7151.

Meek J, Hafmans TG, Maler L, Hawkes R (1992) Distribution of zebrin II in the gigantocerebellum of the mormyrid fish *Gnathonemus petersii* compared with other teleosts. J Comp Neurol 316:17–31.

Miyasaka N, Morimoto K, Tsubokawa T, Higashijima S, Okamoto H, Yoshihara Y (2009) From the olfactory bulb to higher brain centers: genetic visualization of secondary olfactory pathways in zebrafish. J Neurosci 29:4756–4767.

Monsivais P, Clark BA, Roth A, Häusser M (2005) Determinants of action potential propagation in cerebellar Purkinje cell axons. J Neurosci 25:464–472.

Orlovsky GN (1972) Work of the neurons of the cerebellar nuclei during locomotion. Biophysics 17:1177–1185.

Owen SF, Liu MH, Kreitzer AC (2019) Thermal constraints on in vivo optogenetic manipulations. Nat Neurosci 22:1061–1065.

Palkovits M, Mezey E, Hamori J, Szentagothai J (1977) Quantitative histological analysis of the cerebellar nuclei in the cat: I. Numerical data on cells and on synapses. Exp Brain Res 28:189–209.

Person AL, Raman IM (2010) Deactivation of L-type Ca current by inhibition controls LTP at excitatory synapses in the cerebellar nuclei. Neuron 66:550–559.

Person AL, Raman IM (2012a) Purkinje neuron synchrony elicits time-locked spiking in the cerebellar nuclei. Nature 481:502–505.

Person AL, Raman IM (2012b) Synchrony and neural coding in cerebellar circuits. Front Neural Circuits 6:97.

Proville RD, Spolidoro M, Guyon N, Dugué GP, Selimi F, Isope P, Popa D, Léna C (2014) Cerebellum involvement in cortical sensorimotor circuits for the control of voluntary movements. Nat Neurosci 17:1233–1239.

Pugh JR, Raman IM (2006) Potentiation of mossy fiber EPSCs in the cerebellar nuclei by NMDA receptor activation followed by postinhibitory rebound current. Neuron 51:113–123.

Pugh JR, Raman IM (2008) Mechanisms of potentiation of mossy fiber EPSCs in the cerebellar nuclei by coincident synaptic excitation and inhibition. J Neurosci 28:10549–10560.

Raman IM, Bean BP (1999) Ionic currents underlying spontaneous action potentials in isolated cerebellar Purkinje neurons. J Neurosci 19:1663–1674.

Raman IM, Gustafson AE, Padgett D (2000) Ionic currents and spontaneous firing in neurons isolated from the cerebellar nuclei. J Neurosci 20:9004–9016.

Sarnaik R, Raman IM (2018) Control of voluntary and optogenetically perturbed locomotion by spike rate and timing of neurons of the mouse cerebellar nuclei. eLife 7:e29546.

Scalise K, Shimizu T, Hibi M, Sawtell NB (2016) Responses of cerebellar Purkinje cells during fictive optomotor behavior in larval zebrafish. J Neurophysiol 116:2067–2080.

Sengupta M, Thirumalai V (2015) AMPA receptor mediated synaptic excitation drives state-dependent bursting in Purkinje neurons of zebrafish larvae. eLife 4:e09158.

Softky WR, Koch C (1993) The highly irregular firing of cortical cells is inconsistent with temporal integration of random EPSPs. J Neurosci 13:334–350.

Sugihara I, Fujita H, Na J, Quy PN, Li BY, Ikeda D (2009) Projection of reconstructed single Purkinje cell axons in relation to the cortical and nuclear aldolase C compartments of the rat cerebellum. J Comp Neurol 512:282–304.

Takeuchi M, Yamaguchi S, Sakakibara Y, Hayashi T, Matsuda K, Hara Y, Tanegashima C, Shimizu T, Kuraku S, Hibi M (2017) Gene expression profiling of granule cells and Purkinje cells in the zebrafish cerebellum. J Comp Neurol 525:1558–1585.

ten Brinke MM, Boele HJ, Spanke JK, Potters JW, Kornysheva K, Wulff P, IJpelaar AC, Koekkoek SK, De Zeeuw CI (2015) Evolving models of Pavlovian conditioning: cerebellar cortical dynamics in awake behaving mice. Cell Rep 13:1977–1988.

Teune TM, van der Burg J, de Zeeuw CI, Voogd J, Ruigrok TJ (1998) Single Purkinje cell can innervate multiple classes of projection neurons in the cerebellar nuclei of the rat: a light microscopic and ultrastructural triple-tracer study in the rat. J Comp Neurol 392:164–178.

Thach WT (1968) Discharge of Purkinje and cerebellar nuclear neurons during rapidly alternating arm movements in the monkey. J Neurophysiol 31:785–797.

Tomko GJ, Crapper DR (1974) Neuronal variability: non-stationary responses to identical visual stimuli. Brain Res 79:405–418.

Wang WC, McLean DL (2014) Selective responses to tonic descending commands by temporal summation in a spinal motor pool. Neuron 83:708–721.

Witter L, Canto CB, Hoogland TM, de Gruijl JR, De Zeeuw CI (2013) Strength and timing of motor responses mediated by rebound firing in the cerebellar nuclei after Purkinje cell activation. Front Neural Circuits 7:133.

Wylie DR, De Zeeuw CI, DiGiorgi PL, Simpson JI (1994) Projections of individual Purkinje cells of identified zones in the ventral nodulus to the vestibular and cerebellar nuclei in the rabbit. J Comp Neurol 349:448–463.